

Intercomparison of Wave Data ^{*}

Jørg E. Aarnes
SINTEF Applied Mathematics
N-0314 Oslo, Norway

and

Harald E. Krogstad
Dept. Mathematical Sciences, NTNU
N-7491 Trondheim Norway

Abstract

The report addresses techniques and problems encountered during intercomparisons of wave data. Following a general discussion of intercomparing wave data, the basic sea state parameters and spectra are recalled, and various aspects of the sampling variability theory are discussed.

Intercomparing scalar data is typically carried out by means of scatter plots, but when both data are subject to random sampling error, classical regression will produce heavily biased results. The Maximum Likelihood and *Total Least Square* (TLS) regression does not have this shortcoming, and in particular TLS regression is found to be quite suitable if there is some information about the sampling variability, at least for one of the instruments. TLS, also called *Weighted Orthogonal Distance Regression* (WODR) may be rather complex numerically, and here we only show some examples for the case where there is a fixed ratio between the error variances for the two data sets.

The *Quantile-Quantile* (Q-Q) plot is a very simple non-parametric technique that is often used to compare one data set to an assumed theoretical distribution. It is shown that it can be extended to a non-parametric regression when the sampling variabilities for the data are comparable.

Due to the large dynamic range of directional spectra, together with considerable sampling variability, direct comparisons using contour or 3D plots are difficult. Moreover, directionally integrated parameters like the mean direction and the directional spread are not very informative when more than one dominating wave field is present in the spectrum. The best therefore seems to be to apply a spectral partitioning algorithm in order to split a directional spectrum into its main wave fields, and then compare the parameters for each field separately. The report contains a short review of the spectral partitioning techniques.

^{*}This work is a part of work package 1 (Wp4) of the EnviWave (EVG-2001-00017) research programme under the EU Energy, Environment and Sustainable Development program.

Contents

1	Introduction	3
2	General considerations	4
3	Wave Parameters	6
4	The Sampling Variability of Wave Parameters	7
4.1	The frequency spectrum and derived parameters	7
4.1.1	Spatially averaging instruments	10
4.1.2	Intercomparison of frequency spectra	10
4.2	Directional wave parameters	12
4.3	The variability of the directional distribution	14
4.4	Spatial and temporal measurements	15
5	Intercomparisons of Scalar Wave Data	18
5.1	The general setting	18
5.2	Maximum likelihood and Total Least Squares	20
5.2.1	Linear Total Least Squares	21
5.2.2	Angular quantities	23
5.2.3	Further discussion of linear TLS	24
5.3	Nonparametric Techniques	27
5.3.1	Quantile plots as a non-parametric regression	27
6	Intercomparison of Directional Spectra	28
6.1	Conventional Intercomparisons	30
6.2	Spectral Partitioning	31
6.2.1	Isolate the spectral energy peaks	32
6.2.2	Identify and combine wind sea peaks	32
6.2.3	Identify and combine mutual swell peaks	33
6.2.4	Remove low energy partitions	33
6.2.5	Calculate partition statistics	33
6.3	Cross assignment of spectral wave systems	34
7	Conclusions	34

1 Introduction

This report addresses techniques and problems often encountered during intercomparisons of wave data. The most familiar graph for an ocean wave analyst is probably a scatter plot with simultaneous data of significant wave height from two different instruments, e.g. two different buoys, or a satellite and a buoy. The plot is characterized with a cloud of points, and with a scatter that typically increases as the wave height increases. The scatter may for a large part be due to the intrinsic sampling variability of the measurements. Although the sampling variability for *in-situ* measurements is reasonably well known, the theory for satellite data is more incomplete. Thus, assessing the variability of satellite data by comparing to buoy data is not completely straightforward due to the sampling errors also present in the buoy data [22].

The scope of the report is somewhat limited and the statistical procedures are kept at a simple level. In fact, many of the classical statistical tests are not easily applied in the present situation, but in some cases nonparametric tests are suitable.

Following a general discussion of intercomparing wave data, we first recall the basic sea state parameters and spectra, and then proceed to discuss various aspects of the sampling variability theory. It is particularly interesting to see how the sampling variability varies differently for time recording (typically *in situ*) or spatially recording (typically *remote sensing*) instruments.

Intercomparing scalar data is always done by means of scatter plots. A regression line, or more generally a curve, then summarizes the intercomparison and provides a calibration relation between the instruments [3]. In the present case, where both instruments are subject to considerable random sampling error, classical regression will produce heavily biased results. The Maximum Likelihood and *Total Least Square* (TLS) regression does not have this shortcoming, and in particular TLS regression is found to be quite suitable if one has some idea about the sampling variability, at least for one of the instruments. Unfortunately, TLS, also called *Weighted Orthogonal Distance Regression* (WODR) may be rather tricky numerically although computer codes are freely available. In this report we show some examples for the case where there is a fixed ratio between the error variances for the two data sets.

A *Quantile-Quantile* (Q-Q) plot is a very simple non-parametric technique that is usually used to compare one data set to an assumed theoretical distribution. It can be extended to a non-parametric regression when the sampling variabilities are comparable. The Q-Q regression is suitable when data from various instrument sources are merged into a common set for long term wave statistics since in that case, the overall distribution of the data are fitted.

Due to the large dynamic range of directional spectra, together with considerable sampling variability, direct comparisons using contour or 3D plots are difficult. Moreover, directionally integrated parameters like the mean direction and the directional spread are not very informative when more than one dominating wave field is available. The best therefore seems to be to apply a spectral partitioning algorithm in order to split a directional spectrum into its main wave fields, and then compare the parameters for each field separately. A review of the spectral partitioning techniques is included in Sec. 6.

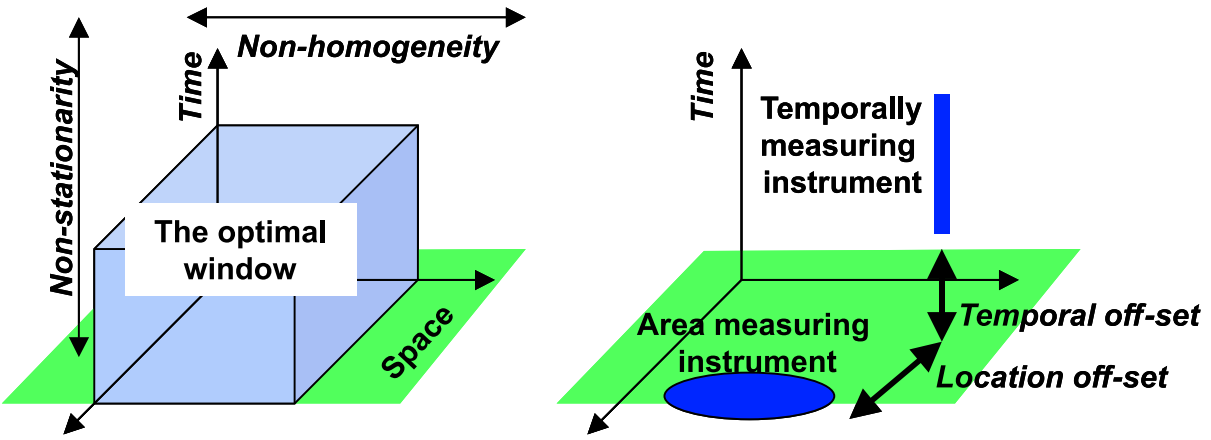


Figure 1: The hypothetical optimal space/time window (taking non-homogeneity and non-stationarity into account), and real wave measuring instruments.

2 General considerations

Intercomparison of wave data highlights the problems encountered in comparing any data sets. The data are often collected from different kinds of instruments, using different sampling strategies and different analysis procedures [22]. The data may be available in the form of directional wave spectra, or in the form of parameters derived from the spectra. Various statistics must be chosen in an optimal way to illustrate similarities and differences between the instruments. An important feature of wave measurements is that nature varies in a stochastic manner beyond our control.

Often wave data from different sources have to be compiled into larger data bases, and in order to obtain a uniform data set, it is necessary to apply calibration relations derived from intercomparison between the instruments. Optimal calibration curves are therefore an important tool for the intercomparisons. Some of the intercomparison techniques that are used to compare different instruments may also be used to compare wave model results with observations [15],[31].

Generally speaking, measurements of ocean waves involve estimation of parameters of random models. A central assumption about the random model is that it is stationary or homogeneous, – a property which is never strictly attained in practice. Even if there are optimal space/time windows in which the wave field is stationary and the parameters can be estimated with maximal accuracy, no instrument existing today is close to reaching such accuracy even for common sea state parameters like the significant wave height. Figure 1 shows some the dilemmas encountered when intercomparing wave data.

Consider two wave instruments recording the same sea states independently, as illustrated in Fig. 2. The basic task will often be to reveal any systematic differences between the instruments, based on the actual measurements and information about the measurement principles and previous experience. Associated with each measurement there are first of all independent *sampling errors*. These sampling errors are often strongly dependent of the underlying sea state. In addition, both instruments have in general *systematic* offsets (e.g. calibration errors), also depending on the sea state. Finally, there may be temporal and spatial offsets between the recordings which result in

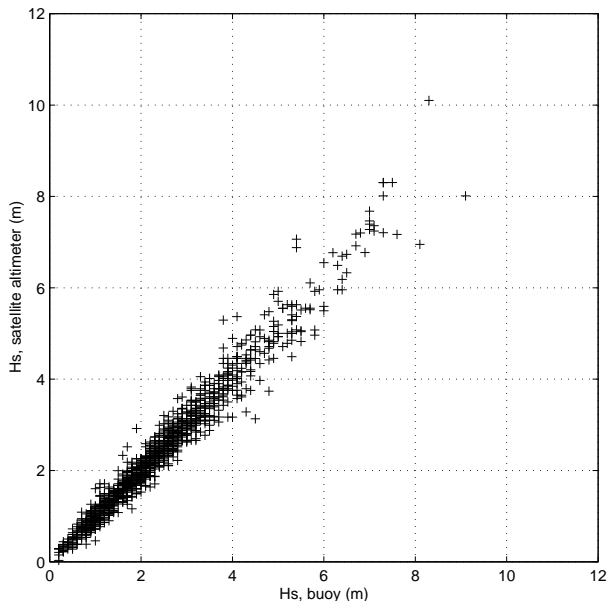


Figure 2: A typical data intercomparison: Buoy *in situ* data *vs.* co-located satellite data.

differences between the actually measured sea states. In addition, the underlying sea states vary according to a certain natural variability which is beyond our control. We are thus facing several potential problems which have to be analysed and resolved properly:

- Possible effects of differences in measurement principles
- Assessment of inherent instrument limitations due to the measurement principles
- Systematic off-sets due to lack of a proper calibration
- Inherent and in general different sampling variability, dependent on the sea state
- Incomplete data coverage due to limited variability of the sea states
- Temporal and/or spatial offsets

Different instruments have different applications and inherent instrument limitations, as long as they are known, may not be a problem. Whereas buoys are known to be excellent for measuring overall sea state parameters, their surface profiling capability (for crest height, wave skewness etc.) is less satisfactory. Sub-surface instrumentation like the current meters/pressure cells or bottom mounted pressure transducers have limited high frequency sensitivity simply because of the wave action attenuation with depth. Spatial arrays are in many respects different from point measurements with a sensitivity that may be dependent both on the frequency and direction of the incoming waves. Also, a spatial array is essentially limited to wave lengths longer than its size. Another feature of spatially extending instruments is that most analysis techniques need to assume linear wave theory. Many remote sensing measurement techniques such as the Synthetic Aperture Radar still suffer from a lack in our basic understanding of the measurement mechanisms. In these

cases there are also limitations due to the resolution which determines the minimum wavelength that can be observed at all.

A proper calibration of the instruments is essential for unbiased measurements, as discussed in [4]. When measuring waves with heave/pitch/roll buoys one typically has to consider several types of calibrations. The heave motion itself has a resonance which depends on the geometry and weight of the buoy. For medium size buoys the resonance is above the main wave frequencies although some resonant enhancement and phase shift may extend into the high frequency range of the wave spectrum. On the contrary, the pitch and roll resonant motion is typically situated at an important range of the wave spectrum. This motion, which can be approximately modelled as an harmonic oscillator driven by a random force, may be strongly out of phase with the actual surface slope. In addition, electronic filters, e.g. integration of acceleration measurements and anti-aliasing filters are frequently involved. As long as the response is linear, it is simple to make corrections by applying appropriate transfer functions to the spectrum, but often one encounters a non-linear response for which it is very difficult to correct.

3 Wave Parameters

We write the ocean surface, $\eta(\mathbf{x}, t)$, in terms of the spectral representation as

$$\eta(\mathbf{x}, t) = \int_{k, \omega} e^{i(\mathbf{k}\mathbf{x} - \omega t)} dZ(\mathbf{k}, \omega), \quad (1)$$

and define the three dimensional spectrum as

$$d\chi(\mathbf{k}, \omega) = \mathbb{E}(dZ(\mathbf{k}, \omega) \overline{dZ(\mathbf{k}, \omega)}).$$

For linear wave theory, the spectrum is supported on the dispersion surface

$$\omega^2 = gk \tanh(kh), \quad (2)$$

where $k = |\mathbf{k}|$, and h is the water depth (in the absence of currents) and the *wavenumber spectrum* is defined by

$$\Psi(\mathbf{k}) d^2k = \int_{\omega > 0} d\chi(\mathbf{k}, \omega).$$

The wavenumber spectrum may be expressed in terms of frequency and direction instead of wavenumber as a *directional spectrum*

$$E(f, \theta) = \Psi(k(f), \theta) k(f) \frac{dk}{df},$$

$$(2\pi f)^2 = gk(f) \tanh(k(f)h).$$

This directional wave spectrum is further written as $E(f, \theta) = S(f)D(\theta, f)$, where S is the frequency spectrum and D the frequency dependent directional distribution expressed as the Fourier series

$$D(\theta, f) = \frac{1}{2\pi} + \frac{1}{\pi} \sum_{n=1}^{\infty} a_n(f) \cos n\theta + b_n(f) \sin n\theta.$$

Table 1 contains a survey of the main sea state parameters[28].

Name	Symbol	Definition
Significant Wave height	H_s	$H_s = 4m_0^{1/2}$, $m_k = \int_{f=0}^{\infty} f^k S(f) df$
Mean zero-crossing period	T_z	$T_z = (m_0/m_2)^{1/2}$
Mean wave period	T_m	$T_m = m_0/m_1$
Peak period	T_p	$T_p = 1/f_p$, $\max_f S(f) = S(f_p)$
Mean Wave Direction	θ_1	$\theta_1(f) = \text{atan } 2(b_1(f), a_1(f))$
Directional spread	σ_1	$\sigma_1(f) = (2(1-r))^{1/2}$, $r = [a_1^2(f) + b_1^2(f)]^{1/2}$
Direction at the spectral peak	θ_p	$\theta_p = \theta_1(f = 1/T_p)$
Spread at the spectral peak	σ_p	$\sigma_p = \sigma_1(f = 1/T_p)$

Table 1: Main sea state parameters

4 The Sampling Variability of Wave Parameters

4.1 The frequency spectrum and derived parameters

The sampling theory for time series, in particular in the spectral domain, is fairly straightforward. The periodogram is the squared magnitude of the discrete Fourier transform of the time series, and the Central Limit Theorem for discrete Fourier transforms ensures that the periodogram values $I(f_k)$ are (scaled) χ^2 -distributed variables with 2 degrees of freedom (DOF). For reasonably long time series, and series with smooth spectra, we may for practical computations assume that

$$\begin{aligned}
\mathbb{E}(I(f_k)) &\approx S(f_k) \\
\text{Var}(I(f_k)) &\approx S(f_k)^2 \\
\text{Cov}(I(f_k), I(f_l)) &= 0, \quad k \neq l
\end{aligned} \tag{3}$$

where $\{f_k\}$ is the discrete set of frequencies for which the periodogram is defined from the discrete Fourier transform. Above *reasonably long* means long compared to the correlation time scale of the series. *Bias* in the periodogram, often called spectral leakage, may be reduced by data tapering. The ocean wave frequency spectrum is fairly smooth and both the recording interval and the sampling frequency for time series data are usually quite satisfactory.

Many of the sea state parameters dependent on the frequency spectrum are derived from the spectral moments defined by

$$m_r = \int_{f=0}^{\infty} f^r S(f) df. \tag{4}$$

The most common estimates for the moments \hat{m}_r , are discrete Riemann sums over the peri-

odogram for which it follows that

$$\begin{aligned}\mathbb{E}(\hat{m}_r) &= m_r, \\ \text{Var}(\hat{m}_r) &= \frac{1}{T} \int_{f=0}^{\infty} f^{2r} S^2(f) df + \mathcal{O}(N^{-2}), \\ \text{Cov}(\hat{m}_r, \hat{m}_s) &= \frac{1}{T} \int_{f=0}^{\infty} f^{r+s} S^2(f) df + \mathcal{O}(N^{-2}),\end{aligned}\tag{5}$$

where T is the recording interval and N the number of points in the time series [21]. In practice, these quantities may also be computed from a discrete sum over a *smoothed* periodogram (spectrum). This smoothed spectrum is also a χ^2 -distributed variable approximately fulfilling

$$\mathbb{E}(\hat{S}(f)) \approx S(f)\tag{6}$$

$$\text{Var}(\hat{S}(f)) \approx (2/\nu)S(f)\tag{7}$$

$$\mathbb{E}(\hat{S}^2(f)) \approx (1 + 2/\nu)S^2(f)\tag{8}$$

where ν is the degrees of freedom, – of the order twice the number of periodogram values involved in the smoothing.

There is a trade-off between the resolution of the smoothed spectrum and the requirement of independent spectral estimates. Obviously, for a sampling frequency f_s , the recording interval is $T = N/f_s$ and the periodogram frequency resolution is f_s/N . The maximum frequency resolution in a smoothed spectrum with ν degrees of freedom which maintains independent spectral estimates is therefore $\Delta f = (\nu/2)f_s/N$.

The Taylor expansion technique is a simple way to obtain the stochastic properties of more complicated expressions of the spectrum. If $\mathbf{X} = (X_1, \dots, X_N)$ is a multivariate stochastic variable for which

$$\text{Var}(X_i) \ll \mathbb{E}(X_i)^2, \quad i = 1, \dots, N,\tag{9}$$

and $\mathbf{Y} = \mathbf{g}(\mathbf{X})$ is a differentiable function, then to the leading order,

$$\mathbb{E}(\mathbf{Y}) = \mathbf{g}(\mathbb{E}(\mathbf{X})), \quad \mathbf{C}_{\mathbf{Y}\mathbf{Y}} = \mathbf{D}\mathbf{C}_{\mathbf{X}\mathbf{X}}\mathbf{D}^t,\tag{10}$$

where $\mathbf{D} = d_{ij}$, $d_{ij} = \{\partial g_i / \partial x_j\}$, and $\mathbf{C}_{\mathbf{X}\mathbf{X}}$ is the variance-covariance matrix of \mathbf{X} , and similarly for \mathbf{Y} .

The Taylor expansion technique may be applied to determine the variance for parameters which are functions of the spectral moments:

$$\begin{aligned}\widehat{Hs} &= 4\hat{m}_0^{1/2}, \quad \text{Var}(\widehat{Hs}) = 4m_{00}/m_0, \\ \widehat{Tm} &= \hat{m}_0/\hat{m}_1, \quad \text{Var}(\widehat{Tm}) = \frac{m_{00}}{m_1^2} - 2\frac{m_0m_{01}}{m_1^3} + \frac{m_0^2m_{11}}{m_1^4}, \\ \widehat{Tz} &= (\hat{m}_0/\hat{m}_2)^{1/2}, \quad \text{Var}(\widehat{Tz}) = \frac{1}{4} \left(\frac{m_{00}}{m_0m_2} - 2\frac{m_{02}}{m_2^2} + \frac{m_0m_{22}}{m_2^3} \right),\end{aligned}\tag{11}$$

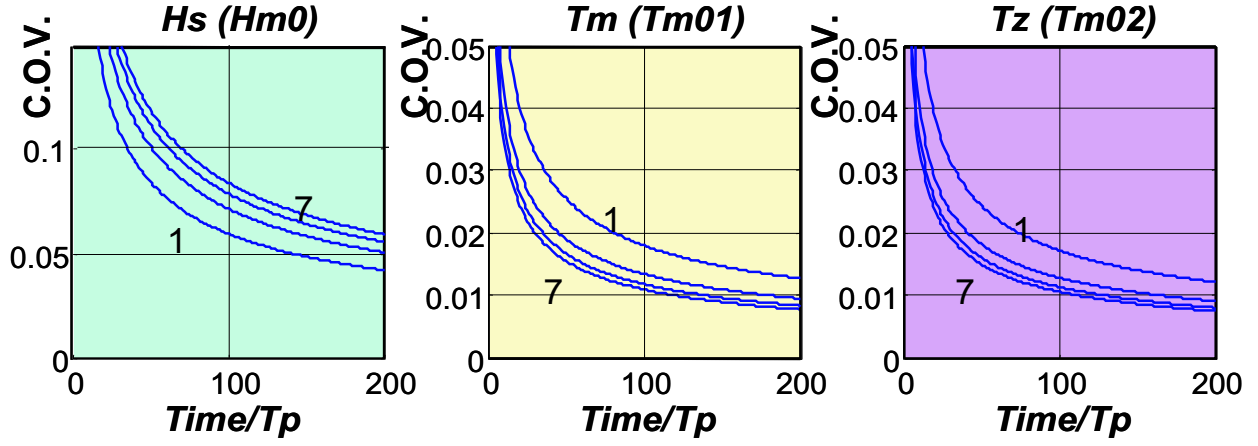


Figure 3: Coefficient of variation (C.O.V.) for three common wave parameters. JONSWAP spectra with high frequency tail asymptotic to $f^{-4.5}$, and γ values 1, 3, 5, and 7 (indicated on the graphs). Duration of time series expressed in terms of peak period, Tp .

where $m_{rs} \equiv \text{Cov}(m_r, m_s)$. In a practical analysis, the estimates of the spectral moments and their covariance are used in the expression for the variance. The sampling variability is illustrated in Fig. 3 for a set of JONSWAP wave spectra. In the graph, C.O.V. denotes the *coefficient of variation*,

$$C.O.V.(X) = \frac{\text{std}(X)}{\mathbb{E}(X)},$$

and the duration of the time series is expressed in dimensionless form.

It is also possible to derive an expression for the variance of the estimate for m_0 for an instantly spatially measuring instrument. We then first observe that the wave number spectrum of the instantaneous surface is

$$\phi(\mathbf{k}) = (\Psi(\mathbf{k}) + \Psi(-\mathbf{k})) / 2. \quad (12)$$

If we scale the two-dimensional periodogram such that $\mathbb{E}(I_X(\mathbf{k}_{mn})) = \phi(\mathbf{k}_{mn})$, $\text{Var}(I_X(\mathbf{k}_{mn})) = \phi^2(\mathbf{k}_{mn})$, the estimate for m_0 is

$$\hat{m}_0 = \frac{(2\pi)^2}{\Delta x \Delta y M N} \sum_{m=-M/2}^{M/2} \sum_{n=-N/2}^{N/2} I_X(\mathbf{k}_{mn}), \quad (13)$$

which leads, as the resolution tends to infinity and the covered area is sufficiently large, to

$$E(\hat{m}_0) = \int_{\mathbf{k}} \phi(\mathbf{k}) d^2 k. \quad (14)$$

For the variance, we note that $I_X(\mathbf{k}_{nm}) = I_X(-\mathbf{k}_{-n,-m})$, but otherwise, periodogram values are reasonably independent. Thus,

$$\text{Var}(\hat{m}_0) = \left(\frac{(2\pi)^2}{\Delta x \Delta y M N} \right)^2 4 \sum_{m=-M/2}^{M/2} \sum_{n=0}^{N/2} \text{Var}(I_X(\mathbf{k}_{nm})) \rightarrow \frac{8\pi^2}{A} \int_{\mathbf{k}} \phi^2(\mathbf{k}) d^2 k. \quad (15)$$

By introducing the wavenumber spectrum and neglecting the cross term $\Psi(\mathbf{k})\Psi(-\mathbf{k})$ we have

$$\text{Var}(\hat{m}_0) = \frac{4\pi^2}{A} \int_k \Psi^2(\mathbf{k}) d^2k. \quad (16)$$

4.1.1 Spatially averaging instruments

For instruments of some spatial extent there is a simple estimate of how the size may affect the spectrum. Again consider the surface spectral representation of the surface,

$$\eta(x, t) = \int_{k, \omega} e^{i(kx - \omega t)} dZ(k, \omega). \quad (17)$$

An ideal instrument situated at the origin measures

$$\eta(0, t) = \int_{k, \omega} e^{-i\omega t} dZ(k, \omega), \quad (18)$$

whereas an instrument averaging over a circular disc with radius r measures

$$\tilde{\eta}(t) = \frac{1}{\pi r^2} \int_{|x| < r} \eta(\mathbf{x}, t) d^2x. \quad (19)$$

It is easily seen that the spectra for $\tilde{\eta}$ and η are connected as

$$S_{\tilde{\eta}\tilde{\eta}}(f) = |T(k(f), r)|^2 S_{\eta\eta}(f), \quad (20)$$

where the wavenumber $k(f)$ is obtained from the dispersion relation and

$$T(k, r) = \frac{2}{r^2} \int_{\rho=0}^r J_0(k\rho) \rho d\rho = \frac{2J_1(kr)}{kr} = \sum_{j=0}^{\infty} (-1)^j \frac{1}{(j+1)2^{2j}(j!)^2} (kr)^{2j}$$

The spectral transfer function as a function of frequency in deep water is given in Fig. 4.

Often also the surface profiling capabilities of the instrument are important. The actual individual wave profiles are used to study the crest height, the wave skewness (vertical and horizontal) and the height/period distributions. The time series are also necessary when comparing higher order statistics of the time series. A well-known example is the unavoidable horizontal buoy motion when measuring high crests. Non-linear response of heave/pitch/roll buoys represents a different problem. It may be very difficult to eliminate these features.

4.1.2 Intercomparison of frequency spectra

When comparing spectra, it is convenient to consider the so-called spectral ratio,

$$r(f) = \frac{S_Y(f)}{S_X(f)}. \quad (21)$$

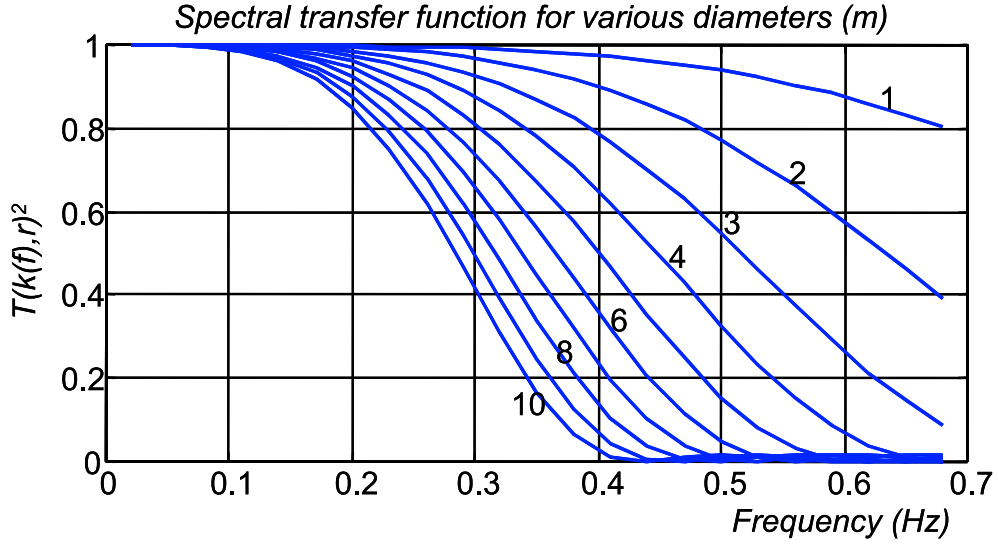


Figure 4: Transfer function for disc averaging instrument in deep water as a function of the diameter of the disc.

When estimating the spectral ratio from measured spectra, it is necessary to apply a bias correcting factor. If the spectra for the two systems have been computed with ν_X and ν_Y degrees of freedom, then the bias free estimate for the spectral ratio is

$$\hat{r}(f) = \frac{\hat{S}_Y(f) \nu_X - 2}{\hat{S}_X(f) \nu_X} \quad (22)$$

This spectral ratio will be a (scaled) Fisher distributed variate with ν_Y and ν_X degrees of freedom and, as such, have a variance equal to

$$\text{Var}(\hat{r}(f)) = \frac{2(\nu_X + \nu_Y - 2)}{\nu_X(\nu_Y - 4)}. \quad (23)$$

An alternative to the ratio is to consider the logarithm of the spectra. Since \hat{S} is distributed according to a scaled χ_ν^2 -distribution, $U = \log(\hat{S}/E(\hat{S}))$ has a distribution which is easily expressed in terms of the χ_ν^2 probability density. The distribution is considerably more symmetric about its mean and in particular,

$$\begin{aligned} \mathbb{E}(U) &= \psi(\nu/2) - \log(\nu/2) \\ \text{Var}(U) &= \psi'(\nu/2) \end{aligned} \quad (24)$$

where $\psi(z) = \Gamma'(z)/\Gamma(z)$ is the di- Γ -function (see Abramowitz and Stegun [1], §26.4.37). From the asymptotic expansion of y , $\psi(z) = \log(z) - \frac{1}{2z} + \frac{1}{12z^2} + \dots$, we obtain

$$\begin{aligned} \mathbb{E}(\log(\hat{S})) &= \log(\mathbb{E}(\hat{S})) - \frac{1}{\nu} + \frac{1}{3\nu^2} + \dots \\ \text{Var}(\log(\hat{S})) &= \frac{2}{\nu} + \frac{2}{\nu^2} + \dots \end{aligned} \quad (25)$$

4.2 Directional wave parameters

Since directional spectral estimation from in-situ data involves computing auto and cross spectra from several time series, the simple theory for single time series does not apply. However, as mentioned above, time series in ocean wave measurements are generally long compared to the typical correlation distance in the series and in addition, the underlying spectra are reasonably smooth (Wind wave spectra from very extreme seas or narrow swell spectra may be somewhat questionable in this respect). Hence, the sampling variability of the cross spectrum estimates is then governed by the complex Wishart distribution (See, *e.g.*, [8]).

The only instrument where a complete asymptotic theory of the sampling variability of the directional parameters exists is the single point triplet. The theory was developed by R.B. Long around 1980 and we shall for completeness recall some of Long's results below [23]. Consider a heave/pitch/roll buoy and let

$$\sigma^T = [\sigma_{hh} \quad \sigma_{xx} \quad \sigma_{yy} \quad \Im(\sigma_{xh}) \quad \Im(\sigma_{yh}) \quad \Re(\sigma_{xy})], \quad (26)$$

$$\mathbf{d}(\sigma) = \begin{bmatrix} a_1 \\ b_1 \\ a_2 \\ b_2 \end{bmatrix} = \begin{bmatrix} \Im(\sigma_{xh})/\sqrt{\sigma_{hh}(\sigma_{xx} + \sigma_{yy})} \\ \Im(\sigma_{yh})/\sqrt{\sigma_{hh}(\sigma_{xx} + \sigma_{yy})} \\ (\sigma_{xx} - \sigma_{yy})/(\sigma_{xx} + \sigma_{yy}) \\ 2\Re(\sigma_{xy})/(\sigma_{xx} + \sigma_{yy}) \end{bmatrix}. \quad (27)$$

By a Taylor expansion of the estimate $\hat{\mathbf{d}}$ around the expectation value, and applying Eqn. 10, we obtain

$$\mathbb{E}(\hat{\mathbf{d}}) = \mathbf{d}, \quad \mathbf{V} = \mathbf{D}\mathbb{E}(\delta\sigma\delta\sigma^T)\mathbf{D}^T = \mathbf{D}\mathbf{U}\mathbf{D}^T. \quad (28)$$

The covariance matrix \mathbf{U} is found by means of the Wishart distribution of $\hat{\Sigma}$ and the elements in \mathbf{V} may be expressed explicitly as in Table 2.

$V_{11} = \frac{1}{2\nu}$	$a_1^2 z_1 - 2a_1 b_1 b_2 - a_2(2a_1^2 - 1) + 1$	
$V_{22} = \frac{1}{2\nu}$	$b_1^2 z_1 - 2a_1 b_1 b_2 + a_2(2b_1^2 - 1) + 1$	
$V_{12} = \frac{1}{2\nu}$	$a_1 b_1 z_1 - b_2(r_1^2 - 1)$	
$V_{13} = \frac{1}{\nu}$	$a_1 a_2 z_2 - a_1(a_1^2 - b_1^2 + a_2^2 - 1) - b_1 b_2(a_2 + 1)$	
$V_{23} = \frac{1}{\nu}$	$b_1 a_2 z_2 - b_1(a_1^2 - b_1^2 - a_2^2 + 1) - a_1 b_2(a_2 - 1)$	
$V_{14} = \frac{1}{\nu}$	$a_1 b_2(z_2 - a_2) - b_1(2a_1^2 + b_2^2 - a_2 - 1)$	
$V_{24} = \frac{1}{\nu}$	$b_1 b_2(z_2 + a_2) - a_1(2a_1^2 + b_2^2 + a_2 - 1)$	
$V_{33} = \frac{1}{\nu}$	$(a_2^2 - 1)(r_2^2 - 1)$	
$V_{44} = \frac{1}{\nu}$	$(b_2^2 - 1)(r_2^2 - 1)$	
$V_{34} = \frac{1}{\nu}$	$a_2 b_2(r_2^2 - 1)$	
$V_{ij} = V_{ji}$		
$z_1 = 2(r_1^2 - 1) + \frac{1}{2}(r_2^2 - 1), z_2 = (r_1^2 - 1) + \frac{1}{2}(r_2^2 + 1)$ $r_1^2 = a_1^2 + b_1^2, r_2^2 = a_2^2 + b_2^2$		

Table 2: Elements of the covariance matrix for estimates of the Fourier coefficients. The numbering 1 - 4, refers to $\hat{a}_1, \hat{b}_1, \hat{a}_2, \hat{b}_2$, respectively. ν is the DOF in the cross spectral estimates.

The statistical properties for the estimates of the directional spread, $\widehat{\sigma}_1$, may be derived by the

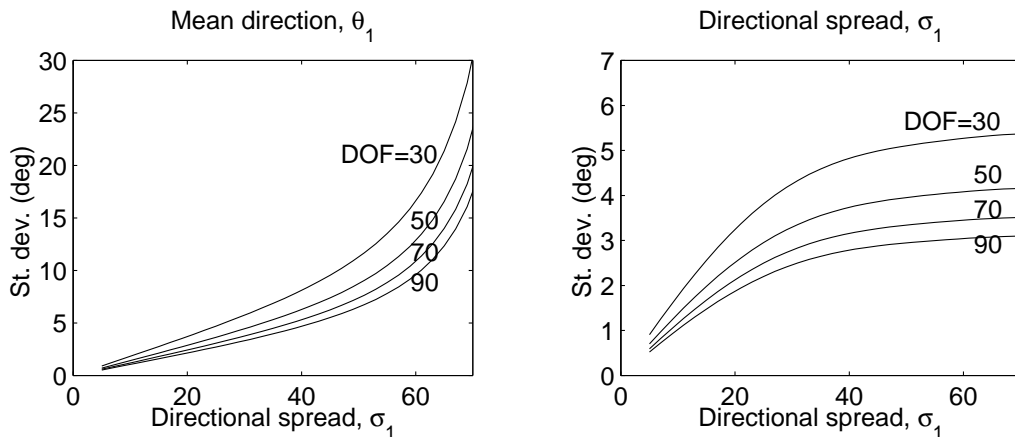


Figure 5: The sampling variability for estimates of the mean direction and the directional spread shown for degrees of freedom (ν) equal to 30, 50, 70, and 90.

same method, utilizing the \mathbf{V} matrix,

$$\text{Var}(\widehat{\sigma}_1) = \frac{1}{2}[(1 - r_1)^3 \text{Var}(s)], \quad (29)$$

where

$$\text{Var}(s) = \frac{1}{(1 - r_1)^4} \left\{ r_1^4 + \frac{1}{4} r_1^2 (r_2^2 - 1) + \left(\frac{1}{2} r_1^{-2} - 1 \right) [r_1^2 + a_2 (a_1^2 - b_1^2) + 2a_1 b_1 b_2] \right\} \frac{1}{\nu}. \quad (30)$$

Similarly, the asymptotic deviation for the mean wave direction is

$$\text{Var}(\theta_1) = \frac{1}{r_1^4} [r_1^2 - a_2 (a_1^2 - b_1^2) - 2a_1 b_1 b_2] \frac{2}{\nu}. \quad (31)$$

The asymptotic sampling variability for estimating the mean direction and the directional spread for a \cos^2 distribution is shown in Fig. 5. It is important to note that the sampling variability is strongly dependent of actual shape of the directional distribution. It is therefore not possible to give a simple answer to questions about the directional resolution of single point triplets.

Modern statistical methods frequently use simulation to reveal the sampling variability. Given the spectral properties, there is a simple and effective way of simulating multivariate Gaussian time series. In this way, it is simple to simulate the output from arbitrary wave recording devices supposing the sea follows Gaussian linear wave theory (see [3]). In some cases it is more convenient to start by simulating the cross spectra directly. Cross spectra of multivariate Gaussian processes have a complex Wishart distribution that is easily simulated by summing the squares of independent complex Gaussian variables [8]. The following conclusions were obtained by a simulation study on the sampling variability of sea state parameters obtained from buoys like the Directional Waverider [25]:

- The asymptotic theory for frequency spectra holds very well
- Variability of parameters derived from the spectrum follows easily and accurately from the Taylor expansion technique using the expression for the variability of the spectral moments.

- The difference between Hs and $H_{1/3}$ (computed from the time series itself) is similar for simulated and real time series, and the sampling variability is similar
- There is a small but significant difference in the expectations of Tz from the spectrum and the time series.
- The variability of Tz is quite small. However, the standard deviation derived from the simulations is about 50% higher for Tz from the time series, as compared to the period computed from the spectrum.
- The standard deviation of Tp is about 4-10 times larger than for Tz .
- For the directional parameters the expressions of R. B. Long seem to be accurate for narrow directional distributions. Some deviations are observed for broad directional distributions.

4.3 The variability of the directional distribution

For directional estimates of the form $D(\theta) = \gamma(\theta)^H \hat{\Sigma} \gamma(\theta)$, where γ is independent of $\hat{\Sigma}$, the sampling variability is simply $\text{Var}(\hat{D}(\theta)) = \frac{2}{\nu} (\mathbb{E} \hat{D}(\theta))^2$ [9]. It has been suggested that a similar expression should be valid in the data adaptive case as well. Unfortunately, this does not appear to be the case. Below we review some results obtained by Ingrid Glad in her masters thesis dealing with the MEM method applied to heave/pitch/roll buoy data [14].

If the theoretical directional distribution is fairly uniform, the Fourier coefficients obtained by the standard method are small, and the ME-directional estimate is to the first order simply the truncated Fourier series:

$$\hat{D}(\theta) \approx \frac{1}{2\pi} \frac{1}{1 - \hat{c}_1 e^{-i\theta} - \hat{c}_1^* e^{i\theta} - \hat{c}_2 e^{-2i\theta} - \hat{c}_2^* e^{2i\theta}} \quad (32)$$

$$\begin{aligned} &\approx \frac{1}{2\pi} (1 + \hat{c}_1 e^{-i\theta} + \hat{c}_1^* e^{i\theta} + \hat{c}_2 e^{-2i\theta} + \hat{c}_2^* e^{2i\theta}) \\ &= \frac{1}{2\pi} (1 + 2(\hat{a}_1 \cos \theta + \hat{b}_1 \sin \theta + \hat{a}_2 \cos 2\theta + \hat{b}_2 \sin 2\theta)). \end{aligned} \quad (33)$$

Moreover, the variance-covariance matrix reduces to

$$\mathbf{V} = \begin{bmatrix} \frac{1}{2\nu} & 0 & 0 & 0 \\ 0 & \frac{1}{2\nu} & 0 & 0 \\ 0 & 0 & \frac{1}{\nu} & 0 \\ 0 & 0 & 0 & \frac{1}{\nu} \end{bmatrix}. \quad (34)$$

The covariance between $\hat{D}(\theta_1)$ and $\hat{D}(\theta_2)$ are then to the leading order

$$\text{Cov}(\hat{D}(\theta_1), \hat{D}(\theta_2)) = \frac{1}{\pi^2} \left(\frac{1}{2\nu} \cos(\theta_1 - \theta_2) + \frac{1}{\nu} \cos 2(\theta_1 - \theta_2) \right).$$

By inserting $\theta_1 = \theta_2$ in the above expression, we obtain

$$\begin{aligned}\text{Var}(\widehat{D}(\theta)) &\approx \left(\frac{1}{\pi}\right)^2 \left(\frac{1}{2\nu} + \frac{1}{\nu}\right) \\ &= \left(\frac{1}{2\pi}\right)^2 \frac{6}{\nu} \\ &= 3 \cdot 2(\mathbb{E}(\widehat{D}(\theta)))^2 / \nu.\end{aligned}\tag{35}$$

Thus, the sampling variability of the MEM-directional estimate for an approximately uniform directional distribution is 3 times the variability of the linear estimates.

It has turned out from computer simulation studies that this result has rather limited validity. For more general distributions an analytical Taylor expansion analysis for the covariance gets very messy. From a series of computer experiments of the variability it was observed that the variability may be substantially larger than for the linear estimates or the MEM-estimate for nearly uniform distributions.

4.4 Spatial and temporal measurements

We are going to investigate the sampling variability of temporal vs. spatial measurements and consider the following two hypothetical instruments. Instrument **A** measures a time series of surface elevation in a single point for a duration T . Instrument **B** measures the elevation of the surface at a fixed instant of time for all points over an area A (In the following derivation we first assume the area to be square, but replace it later with an equivalent disc of diameter d). Both instruments have infinitely high resolution and the sampling interval and area are both large enough for the asymptotic sampling theory to apply. It is convenient to write the wave spectrum in the normalized form

$$S(f)D(\theta, f) = \frac{Hs^2}{16f_p} S_0(f/f_p) D_0(\theta, f/f_p),\tag{36}$$

where $f_p = 1/Tp$, and

$$\int_{x=0}^{\infty} S_0(x) dx = \int_{\theta=0}^{2\pi} D_0(\theta, x) d\theta = 1.\tag{37}$$

Deep water is assumed for simplicity (very shallow water gives actually somewhat different conclusions and is left to the reader).

We consider the estimation of the significant wave height obtained from estimates of the zeroth spectral moment m_0 . As discussed above, when the sampling frequency $f_0 \rightarrow \infty$ and the recording interval T is sufficiently large,

$$\mathbb{E}(\hat{m}_0) = m_0,\tag{38}$$

$$\text{Var}(\hat{m}_0) = \frac{1}{T} \int_{f=0}^{\infty} S^2(f) df.\tag{39}$$

Since $\text{Var}(Hs) = 4 \text{Var}(m_0)/m_0$, we have for the coefficient of variation, C.O.V.,

$$\text{C.O.V.}_{time} = \frac{\text{Std}(Hs)}{Hs} = \frac{\sqrt{\text{Var}(\hat{m}_0)}}{2m_0} = \frac{1}{2} \|S_0\|_2 (f_p T)^{-1/2},\tag{40}$$

where $\|S_0\|_2$ is defined as $(\int S_0(x)^2 dx)^{1/2}$. This is a reasonable expression since the recording length is measured by the time scale f_p^{-1} , the coefficient of variation decreases with the square root of the length of the recording interval, and the norm $\|S_0\|_2$ is a suitable measure of the spectral width, which increases as the spectra get narrower (note that $\int_0^\infty S_0(x) dx = 1$).

For the spatial instrument we showed above that

$$\text{Var}(\hat{m}_0) = \frac{4\pi^2}{A} \int_k \Psi^2(\mathbf{k}) d^2k. \quad (41)$$

Now,

$$\Psi(\mathbf{k})^2 k dk d\theta = S(f)^2 D(\theta, f)^2 \frac{df}{k dk} df d\theta, \quad (42)$$

which leads to

$$\text{Var}(\hat{m}_0) = \frac{4\pi^2}{A} \frac{g^2 H s^4}{2(2\pi)^4 16^2 f_p^4} \int_{x=0}^{\infty} S_0(x)^2 \frac{1}{x^3} \|D(\cdot, x)\|_2^2 dx. \quad (43)$$

If we for simplicity replaces the square area by a disc such that $A = \pi(d/2)^2$, and include, as is common, a 2π factor in the definition of the $\|\cdot\|_2$ -norm for D , define $\lambda_p = (g/2\pi)f_p^{-2}$, and assumes that S_0 is reasonably peaked, we may write the coefficient of variation for Hs simply as

$$\text{C.O.V.}_{space} = \frac{\text{std}(Hm_0)}{Hm_0} = \|D_0(\cdot, 1)\|_2 \|S_0\|_2 (d/\lambda_p)^{-1} \quad (44)$$

The variability is thus inversely proportional to the square root of the measured area, where length is measured by the length scale λ_p . As for the temporal case, the peakedness of the frequency spectrum is important, and in addition, and somewhat interestingly, a *narrow* directional distribution gives larger sampling variability. All this features are actually expected since they reflect the covariance properties of the wave field.

It is interesting to note that if the peak period $T_p = 1/f_p$ increases by a factor of two, the temporal C.O.V. increases by a modest factor $\sqrt{2}$, whereas the spatial C.O.V. increases by a factor 4. In order to keep the same C.O.V.s, one needs to double the registration time T for the temporal instrument but make the registration area 16 times larger for the spatial instrument! On the contrary, if we want to double the precision in our estimates, we only need to double d , whereas a four-fold increase is necessary for T .

If we consider a typical JONSWAP-like frequency spectrum for S_0 and a cos-2s-distribution with $s = 10$ at Tp for D , the corresponding 2-norms come out as $\|S_0\|_2 = 1.03$, $\|D_0(\cdot, s = 10)\|_2 = .32$, see Fig. 6 (Note that a 2π -factor was included in the definition of $\|D_0\|_2$). In this case, we thus obtain the expressions

$$\begin{aligned} \text{C.O.V.}_{time} &\approx .52 (T/T_p)^{-1/2}, \\ \text{C.O.V.}_{space} &\approx .33 (d/\lambda_p)^{-1}. \end{aligned} \quad (45)$$

For a certain C.O.V., the necessary time interval and diameter of the measurement disc are given

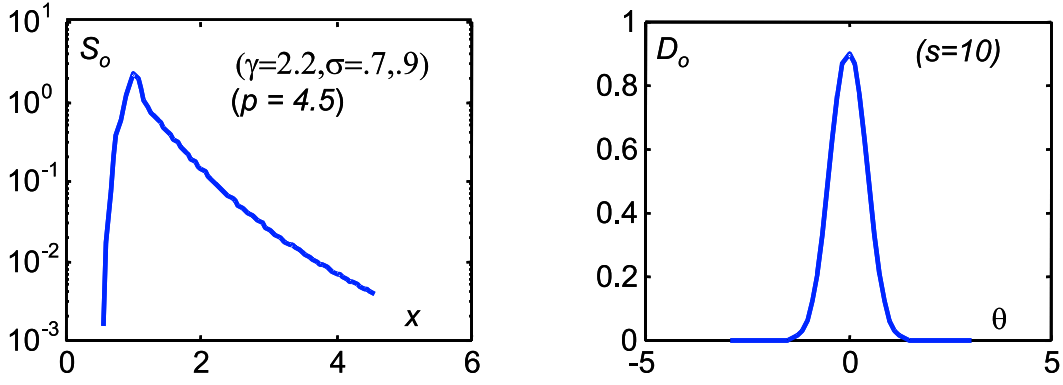


Figure 6: Dimensionless spectra used in the numerical example.

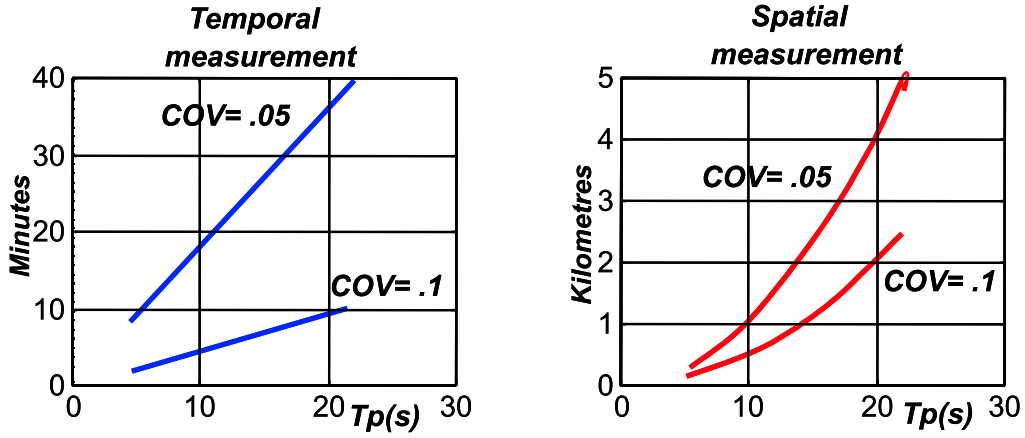


Figure 7: Necessary recording time interval (left) and disc diameter (right) for a given C.O.V. as a function of T_p .

by

$$\begin{aligned}
 T &= \left(\frac{.52}{\text{C.O.V.}_{\text{time}}} \right)^2 T_p, \\
 d &= \frac{.33}{\text{C.O.V.}_{\text{space}}} \frac{g}{2\pi} T_p^2.
 \end{aligned} \tag{46}$$

The relations are shown graphically in Fig. 7.

The satellite radar altimeter measures over an area (including the averaging over partly overlapping discs) of approximately 9km^2 . Similarly, the Envisat Wave Mode spectra are based on imagettes of approximately 63km^2 . The maximal (and highly hypothetical!) maximum precisions in the measurements are then shown in Fig. 8. These lower bounds will hardly ever be of interest for the SAR, but may be of importance for the altimeter at very high sea states.

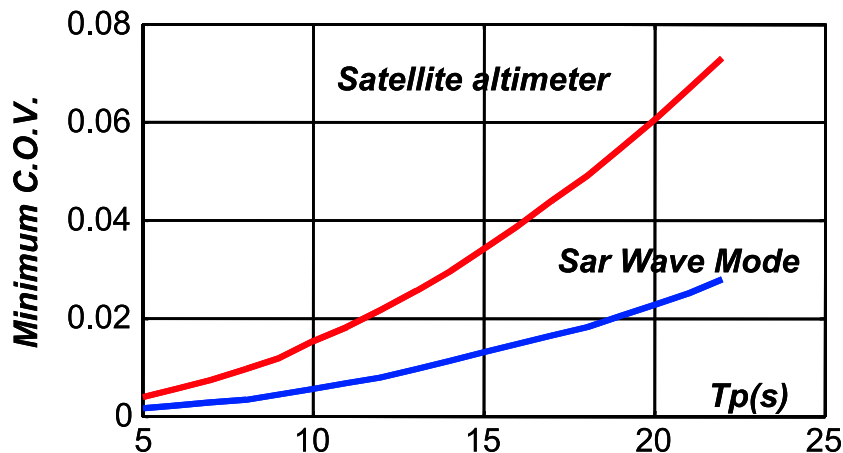


Figure 8: Application of relation to the radar altimeter and the SAR

5 Intercomparisons of Scalar Wave Data

5.1 The general setting

Consider independent and, for simplicity, scalar measurements X and Y of one common wave parameter, μ . The parameter could, *e.g.* be the significant wave height, H_s , measured by a buoy (X) and a satellite altimeter (Y). In general, X and Y suffer from both *systematic* and *sampling* errors. This may be expressed as

$$\begin{aligned}\mathbb{E}(X) &= h(\mu), \\ \mathbb{E}(Y) &= f(\mu),\end{aligned}\tag{47}$$

where $h(\mu)$ and $f(\mu)$ represent systematic off-sets in the measurements of the underlying wave parameter μ . Since we do not know μ exactly, it would in general be impossible determine both $h(\mu)$ and $f(\mu)$. In the following we therefore assume that $h(\mu) = \mu$, and write x for μ , and y for $f(x)$. The primary objective of the data intercomparisons is often to determine the function f or its inverse, since this would be the calibration function to apply if we trust one system more than the other.

At first sight, finding $y = \mathbb{E}(Y) = f(x)$ appears to be a familiar regression problem where $f(x)$ is often assumed to be in the form of a line, $y = \alpha + \beta x$. However, regular regression assumes that the independent variable, say x , is totally free of error, with only Y subject to stochastic variations. In the present case, both X and Y are subject to sampling errors. In addition, these sampling errors tend to depend quite strongly on x . We shall assume that the sampling variability variances $\sigma_x^2(x)$ and $\sigma_y^2(y)$ are functions of x and y . In some cases the sampling variability is essentially known, in other cases it has to be inferred from the data. In order to proceed, we shall therefore assume that the sampling errors are independent from record to record, as well as between the two instruments. This is often quite obvious and a minor restriction. Next, we assume that the sampling errors are Gaussian and, for the moment, that the variances are known functions of x

and y . In practice, this may be true to a larger or smaller extent. The probability laws of X and Y are then

$$\begin{aligned}\mathcal{L}(X) &= \mathcal{N}(x, \sigma_x^2(x)), \\ \mathcal{L}(Y) &= \mathcal{N}(f(x), \sigma_y^2(f(x))).\end{aligned}\tag{48}$$

When the sea state varies, x varies according to a certain density of occurrence π , which, for a long series of observations approaches what is commonly known as the *long term distribution* of x . The observations $(X_i, Y_i)_{i=1}^N$ will thus be obtained from a joint density of the form

$$\phi(\xi, \eta) = \int_s g_X(\xi, s, \sigma^2(s)) g_Y(\eta, f(s), \tau^2(f(s))) \pi(s) ds\tag{49}$$

where g_X and g_Y are Gaussian densities,

$$g(\xi) = \frac{1}{\sqrt{2\pi}\sigma(x)} e^{-(\xi-x)^2/2\sigma(x)^2}.\tag{50}$$

Note that the density in Eqn. 49 is in general *not* a bi-variate Gaussian density. The primary aim will often be to determine the function $f(x)$, although unbiased estimates of the distribution π may be of independent interest.

The above situation suggests what is called an *errors-in-variables model* [12]

$$\begin{aligned}X_i &= x_i + \delta_i, \\ Y_i &= f(x_i) + \varepsilon_i, \quad i = 1, \dots, N,\end{aligned}\tag{51}$$

where x_i are unknown and $\mathcal{L}(\delta_i) = \mathcal{N}(0, \sigma_i^2)$, $\mathcal{L}(\varepsilon_i) = \mathcal{N}(0, \tau_i^2)$. One feature of such models is that they are *symmetric* in the sense that as long as f is one-to-one, the result of applying the model to some data is independent of which variables are chosen to be X or Y . Errors-in-variables models have attained a lot of research, but often the error is assumed to be independent of the underlying, or *hidden* variable. This simplifies the theoretical analysis, but is far from the situation in the present case.

An error-in-variable model in which the underlying variables (x, y) are deterministic is called a *functional relationship model*. If (x, y) are random variables, the model is referred to as a *structural relationship model* (Anderson, 1984). In the present case, we have no way of controlling (x, y) , and the stochastic nature of the wave variability makes it natural to consider this as a *structural relationship model*.

Errors-in-variables models have been used in comparisons between HF radar and buoy measurements; see Sova [27] for a functional relationship model, and Samset *et al.* [26] for a structural relationship model.

The varying sampling variability makes a straightforward application of the existing theory not readily applicable, but our scope is limited, and we refer to the literature for a more extensive analysis of error-in-variable models [10],[12].

5.2 Maximum likelihood and Total Least Squares

Assume that the function $y = f(x)$ is parametrized in terms of a set of parameters $\mathbf{p} = \{p_1, \dots, p_k\}$, such that $y = f(x, \mathbf{p})$. For the linear model $y = \alpha + \beta x$, and $\mathbf{p} = \{\alpha, \beta\}$. Since the master distribution (Eqn. 49) is based on normal densities, a *Maximum Likelihood* (ML) approach is natural [27], and the negative logarithm of the log-likelihood function, when we do not consider the x -es to be stochastic, will simply be

$$-\log L(\mathbf{p}, \mathbf{x}|\mathbf{X}, \mathbf{Y}) \sim \sum_{n=1}^N \left\{ \log [\sigma_x(x_n)^2 \sigma_y(f(x_n, \mathbf{p}))^2] + \frac{(X_n - x_n)^2}{\sigma_x(x_n)^2} + \frac{(Y_n - f(x_n, \mathbf{p}))^2}{\sigma_y(f(x_n, \mathbf{p}))^2} \right\}. \quad (52)$$

However, since $\{x_n\}_{i=1}^N$ are not explicitly known, the model has $N + \text{card}(\mathbf{p})$ parameters. For a given set \mathbf{p} , the optimal x_n -s are found by one-dimensional minimization, which for the simplest cases may be found analytically.

It should, however, be observed that Eqn. 52 does not really take into account the underlying distribution of the x -s. This will to some extent introduce a bias in the estimated values of x_n for observations from rapidly varying parts of the $\pi(x)$ -distribution. A-priori information about π could be incorporated into an extended Bayesian approach, and in the present case we apply a *uniform prior*.

Typically, the logarithmic term will be slowly varying, and if this term is omitted completely, the rest of the functional,

$$J(\mathbf{p}|\mathbf{X}, \mathbf{Y}) = \sum_{n=1}^N \left\{ \frac{(X_i - x_n)^2}{\sigma_x(x_n)^2} + \frac{(Y_n - f(x_n, \mathbf{p}))^2}{\sigma_y(f(x_n, \mathbf{p}))^2} \right\}, \quad (53)$$

reduces to what is called *Total Least Squares* (TLS) or *Weighted Orthogonal Distance Regression* (WODR). The TLS expression is appealing from a practical point of view since it is somewhat simpler than the ML-functional and the weights of the observations are scaled by their reliability. Moreover, the relation is dimensionless. If σ_x and σ_y are equal and constant, the expression reduces to the regular Euclidean orthogonal distances to the regression curve. This this also known as *Principal Axes Regression*.

We may, alternatively, write Eqn. 53 in the equivalent form

$$\min \sum_{n=1}^N \frac{1}{\sigma_x^2(x_n)} \left((X_n - x_n)^2 + \gamma(x_n) (Y_n - f(x_n, \mathbf{p}))^2 \right) \quad (54)$$

where $\gamma(x_n)$ is the *variance ratio*,

$$\gamma(x_n) = \frac{\sigma_x(x_n)^2}{\sigma_y(f(x_n, \mathbf{p}))^2}. \quad (55)$$

Even the TLS functional has $N + \text{card}(\mathbf{p})$ unknowns, and the minimization needs in general to be carried out using a suitable numerical algorithm. It may be convenient to use a double iteration where the outer loop seeks the minimum of the functional over the domain of \mathbf{p} , whereas the inner loop solves for x_n , $n = 1, \dots, N$.

Highly efficient algorithms for the ODR problem have been published [6],[7], and the Fortran program suite ODRPACK is available from <http://www.netlib.org>. The idea is to write the functional as a nonlinear unconstrained least square optimization problem in the form

$$J(\mathbf{p}, \mathbf{x}) = \|\mathbf{g}(\mathbf{x}, \mathbf{p})\|_2^2, \quad (56)$$

where \mathbf{g} is the $2N$ -dimensional vector defined as

$$g_n(\mathbf{x}, \mathbf{p}) = \frac{Y_n - f(x_n, \mathbf{p})}{\sigma_{yn}}, \quad g_{N+n}(\mathbf{x}, \mathbf{p}) = \frac{X_n - x_n}{\sigma_{xn}}, \quad n = 1, \dots, N. \quad (57)$$

Note that σ_{xn} and σ_{yn} are constant weights in this formulation, e.g. $\sigma_{xn} = \sigma(X_n)$. By setting $\theta = (\mathbf{p}, \mathbf{x})$, the problem turns into

$$\min_{\theta} \|\mathbf{g}(\theta)\|_2^2, \quad (58)$$

of which there are many well-known and highly effective algorithms. In the present case, the algorithm is an adapted Levenberg-Marquard-algorithm utilizing the rather simple form of the Jacobian $\partial \mathbf{g} / \partial \theta$ [6].

5.2.1 Linear Total Least Squares

The linear regression function is an important special case, and in this case the parameter set p consists of the parameters (α, β) defining the straight line $y = \alpha + \beta x$. The functional takes the form

$$\min \sum_{n=1}^N \frac{1}{\sigma_x^2(x_n)} \left((X_n - x_n)^2 + \gamma(x_n) (Y_n - \alpha - \beta x_n)^2 \right). \quad (59)$$

The solution gives, contrary to regular linear regression, a regression line which is independent of which variable is chosen as X and Y . That is, the pairs

$$\{x_n, y_n = \alpha + \beta x_n\}_{n=1}^N \quad (60)$$

may alternatively be written

$$\{x_n = \tilde{\alpha} + \tilde{\beta} y_n, y_n\}_{n=1}^N \quad (61)$$

where

$$\tilde{\alpha} = -\frac{\alpha}{\beta}, \quad \tilde{\beta} = \frac{1}{\beta}. \quad (62)$$

We first observe that for a given set $\{\alpha, \beta\}$, the minimization of the functional splits into N one-dimensional minimizations. However, the minimization for x_n has to be carried numerically apart from the very simplest cases. For the limiting case when γ tends to 0 or to ∞ we have the obvious solutions:

$$\lim_{\gamma \rightarrow 0} x_n = X_n = x_n^0, \quad (63)$$

$$\lim_{\gamma \rightarrow \infty} x_n = \frac{Y_n - \alpha}{\beta} = x_n^\infty. \quad (64)$$

When the variances are constant, the limiting cases correspond to one-sided regression with respect to X and Y , respectively. It seems obvious that the minimum should be obtained for an x_n in the

interval defined by x_n^0 and x_n^∞ , but it is actually possible to construct cases where σ_x and γ varies in such a way that the minimum is outside this interval, or we may even have multiple solutions. Nevertheless, in practice σ_x and γ are well-behaved smooth functions, and the minimum is found in the interval defined by x_n^0 and x_n^∞ .

When σ_{x_n} and γ_n are constants we find, by taking the derivative of term n in Eqn. 59, that

$$x_n = \frac{X_n + \beta\gamma(Y_n - \alpha)}{1 + \beta^2\gamma} = \frac{1}{1 + \beta^2\gamma}x_n^0 + \frac{\beta^2\gamma}{1 + \beta^2\gamma}x_n^\infty. \quad (65)$$

If the solutions for $\{x_n\}$ in Eqn. 65 are inserted into Eqn. 59, one obtains after some manipulations the expression

$$\sum_{n=1}^N \frac{(Y_n - \alpha - X_n\beta)^2}{(1 + \beta^2\gamma)}. \quad (66)$$

Taking the derivative with respect to α leads at once to

$$\hat{\alpha} = \bar{Y} - \bar{X}\hat{\beta}, \quad (67)$$

where

$$\bar{X} = \frac{1}{N} \sum_{n=1}^N X_n, \quad \bar{Y} = \frac{1}{N} \sum_{n=1}^N Y_n. \quad (68)$$

The derivative with respect to β then gives

$$\sum_{n=1}^N (X_n\beta - Y_n + \alpha)(\beta\gamma Y_n + X_n - \alpha\beta\gamma) = 0. \quad (69)$$

By expanding this expression and introducing the shorthand notation

$$s_{xy} = \frac{1}{N} \sum_{n=1}^N (X_n - \bar{X})(Y_n - \bar{Y}), \quad (70)$$

etc., we obtain a second order equation for β ,

$$\begin{aligned} & (s_{xy} + \bar{X}\bar{Y})\beta^2\gamma + (s_{xx} + \bar{X}\bar{X})\beta - \beta\gamma(s_{yy} + \bar{Y}\bar{Y}) - (s_{xy} + \bar{X}\bar{Y}) + \alpha\beta\gamma\bar{Y} + \alpha\bar{X} \\ & = \beta^2\gamma s_{xy} + \beta s_{xx} - \beta\gamma s_{yy} - s_{xy} = 0. \end{aligned} \quad (71)$$

In summary,

$$\begin{aligned} \hat{\beta} &= \frac{\gamma s_{yy} - s_{xx} + \sqrt{(s_{xx} - \gamma s_{yy})^2 + 4\gamma s_{xy}^2}}{2\gamma s_{xy}}, \\ \hat{\alpha} &= \bar{Y} - \hat{\beta}\bar{X}, \\ x_n &= \frac{X_n + \hat{\beta}\gamma(Y_n - \hat{\alpha})}{1 + \hat{\beta}^2\gamma}. \end{aligned} \quad (72)$$

(See [12] and [2]). The expression reduces to principal axes regression for $\gamma = 1$.

In practice, the variances σ_x^2 and σ_y^2 are seldom known with very large accuracy, and it may therefore be a reasonable approximation to use

$$\begin{aligned}\sigma_x^2(x_n) &\approx \sigma_x^2(X_n), \\ \gamma(x_n) &\approx \frac{\sigma_x(X_n)^2}{\sigma_y(Y_n)^2}.\end{aligned}\tag{73}$$

In fact, this would be pilot estimates for σ_x and γ , which, if necessary, could be replaced by the estimates $\sigma_x(\hat{x}_n)$ and $\sigma_y(\hat{\alpha} + \hat{\beta}\hat{x}_n)$ for a second round. Since both σ_x and γ are constants during the minimization, the determination of x_n is still straightforward and the solution for x_n is easily seen to be the same as Eqn. 65, and if this is inserted into Eqn. 59, the result is

$$\sum_{n=1}^N \frac{\gamma_n}{\sigma_{x_n}^2} \frac{(-X_n\beta + Y_n - \alpha)^2}{1 + \beta^2\gamma_n}.\tag{74}$$

Taking the derivative with respect to α leads again to $\hat{\alpha} = \bar{Y} - \bar{X} \hat{\beta}$, where now \bar{X} and \bar{Y} are weighted means with weights

$$w_n = \frac{\gamma_n}{\sigma_{x_n}^2 (1 + \beta^2\gamma_n)}, \quad n = 1, \dots, N.\tag{75}$$

In general, no simple expression is obtained if this is inserted into Eqn. 74 for a final determination of $\hat{\beta}$. However, if γ may be taken as a constant, the solution will be similar to Eqn. 72 with $s_{xy} = \sum_{n=1}^N w_n (X_n - \bar{X})(Y_n - \bar{Y})$, etc.

This version of TLS is easy to apply and has several interesting properties as will be summarized in Sec. 5.2.3.

5.2.2 Angular quantities

The above formulation for angular data like the wind and wave directions is different since such data have to be combined mod(2π). For a valid linear relationship between two angular variables of the form

$$y = \alpha + \beta x \text{ mod}(2\pi),\tag{76}$$

β can only take the values 1, 0 or -1 , and even in the general case more general case, if $y = f(x, \mathbf{p})$ is supposed to be a smooth function, we need to require that f along with all its derivatives is continuous across 0.

The natural error distributions for directional data is the *von Mises distribution*, the circular analogue of the normal distribution (Mardia, 1972). It has a probability density function v defined by

$$v(x, \mu, \kappa) = (2\pi I_0(\kappa))^{-1} e^{\kappa \cos(x-\mu)}, \quad 0 \leq x < 2\pi, \quad 0 \leq \mu < 2\pi, \quad \kappa > 0.\tag{77}$$

where μ is the *mean direction*; κ is the *concentration parameter*; and I_0 is the modified Bessel function of the first kind of order 0. For $\kappa \rightarrow 0$, the distribution approaches the uniform distribution, whereas for large κ , approach a Normal distribution with mean μ and variance $\sigma^2 = \kappa^{-1}$.

With errors distributed according to $\mathcal{L}(\delta_i) = vM(\cdot, 0, \kappa)$, $\mathcal{L}(\varepsilon_i) = vM(\cdot, 0, \nu)$, the log likelihood for $\beta = 1$ is

$$\log L(\alpha, \mathbf{x}|\mathbf{X}, \mathbf{Y}) \sim \sum_{i=1}^N \{-\log(I_0(\kappa)I_0(\nu)) + \kappa \cos(X_i - x_i) + \nu \cos(Y_i - x_i - \alpha)\}. \quad (78)$$

In the angular case, an assumption of a constant variance is more realistic than in the linear case, and with constant κ and ν and $\gamma = \nu/\kappa$, the problem reduces to the angular version of TLS,

$$\max_a \left\{ \sum_{i=1}^N \{\cos(X_i - x_i) + \gamma \cos(Y_i - x_i - \alpha)\} \right\} \quad (79)$$

The optimal x_i for a fixed value of a is easily seen to be

$$x_i = X_i + \arg\left(1 + \gamma e^{i(Y_i - X_i - \alpha)}\right), \quad i = 1, \dots, N, \quad (80)$$

which for $\gamma = 1$, simplifies to

$$x_i = \frac{Y_i + X_i - \alpha}{2}. \quad (81)$$

The ML estimate (and actually what would be the naturally TLS) for α when $\gamma = 1$ is then

$$\hat{\alpha}_{\gamma=1} = 2 \arg\left(\sum_{i=1}^N \exp\left(i \frac{Y_i - X_i}{2}\right)\right). \quad (82)$$

For a general γ , α needs to be found numerically.

5.2.3 Further discussion of linear TLS

The linear TLS with a constant variance ratio $\gamma = \sigma_{xx}^2/\sigma_y^2$ includes ordinary Y -on- X regression for $\gamma = 0$, Principal Axis Regression for $\gamma = 1$, and X -on- Y regression when $\gamma = \infty$.

All regression lines pass through the point (\bar{X}, \bar{Y}) , and in fact, $\hat{\beta}_\gamma \in \text{int}[\hat{\beta}_o, \hat{\beta}_\infty]$. This may be seen from an inspection of the second order equation for β ,

$$\beta^2 \gamma s_{xy} + \beta s_{xx} - \beta \gamma s_{yy} - s_{xy} = 0. \quad (83)$$

As is well known, $|\hat{\beta}_o| < |\hat{\beta}_\infty|$, and the difference in slope is significant when the scatter is large. This is illustrated for two sets of simulated data in Fig. 9. The simulation is carried out by first generating independent Weibull observations $\{x_n\}$ and define $y_n = x_n$, $n = 1, \dots, N$. Then random Gaussian errors are added,

$$\begin{aligned} X_n &= x_n + \sigma(x_n) e_n, \\ Y_n &= y_n + \gamma \sigma(x_n) e'_n, \end{aligned} \quad (84)$$

where e_n, e'_n are independent $\mathcal{N}(0, 1)$ variables and $\sigma(x_n) = p \cdot x_n$. A standard deviation equal to a fixed fraction of the value, that is, a relative error equal to p , is typical for in-situ time series wave data.

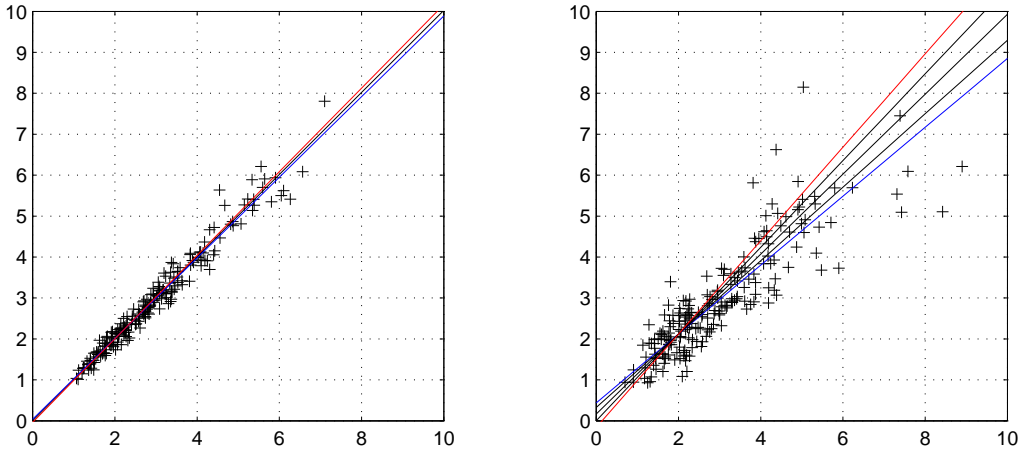


Figure 9: Example of 200 simulated Weibull distributed data with relative error (STD) 5% in both variables (left) and 15% (right). In this case $\gamma = 1$, and the TLS line is the middle line on both graphs. In addition, the left and the right graphs show X -on- Y and Y -on- X , and the right graph even lines for the (wrong) assumptions $\gamma = 3$ and $\gamma = 0.3$.

It is important to observe that the regression line as well as $\{\hat{x}_n\}$ are independent of a uniform scaling of the error variances as long as γ is kept constant. This invariance to the absolute error level makes it impossible to use the analysis to assess the sampling error when nothing is known a priori. We also observe that

$$Y_n - \hat{y}_n = Y_n - \hat{\alpha} - \hat{\beta}\hat{x}_n = \frac{Y_n - \hat{\alpha} - \hat{\beta}X_n}{1 + \hat{\beta}^2\gamma} = -\frac{1}{\hat{\beta}\gamma} (X_n - \hat{x}_n). \quad (85)$$

Let us now consider a somewhat simplified analysis under the assumption that the estimation errors of α and β are negligible. It is then easy to prove that

$$\mathbb{E}(X_n - \hat{x}_n) = 0, \quad (86)$$

$$\text{Var}(X_n - \hat{x}_n) = \sigma_{xn}^2 \frac{\beta^2\gamma}{1 + \beta^2\gamma}, \quad (87)$$

$$\text{Var}\hat{x}_n = \sigma_{xn}^2 \frac{1}{1 + \beta^2\gamma}. \quad (88)$$

The estimate \hat{x}_n has a reduced scatter compared to X_n . This is to be expected since \hat{x}_n is a combination of X_n and Y_n .

The expression for the variance of $X_n - \hat{x}_n$ may be used to check the assumptions about the error. According to Eqn. 87, the normalized variable

$$Z_n = \frac{X_n - \hat{x}_n}{\sigma_{xn}} \sqrt{\frac{1 + \beta^2\gamma}{\beta^2\gamma}} \quad (89)$$

has expectation 0 and standard deviation 1, which is easy to inspect for a set of bins covering the X -range.

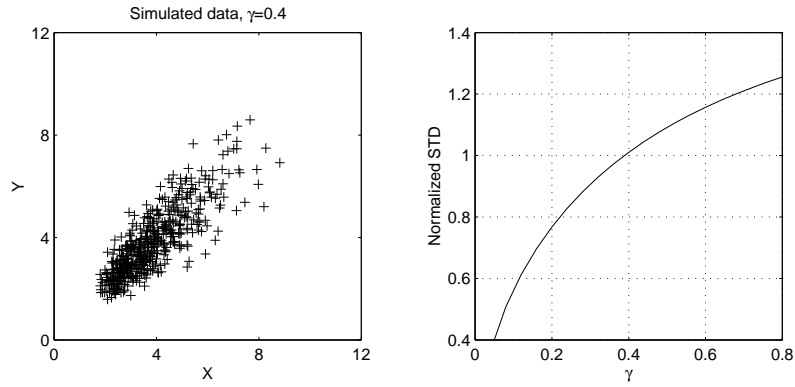


Figure 10: Estimation of the variance ratio. The relative standard deviation in the X -values is 5%, and with $\gamma = 0.4$, 12.5% in the Y -values. $N = 500$ independent samples. The correct value is spotted quite well in the graph to the right.

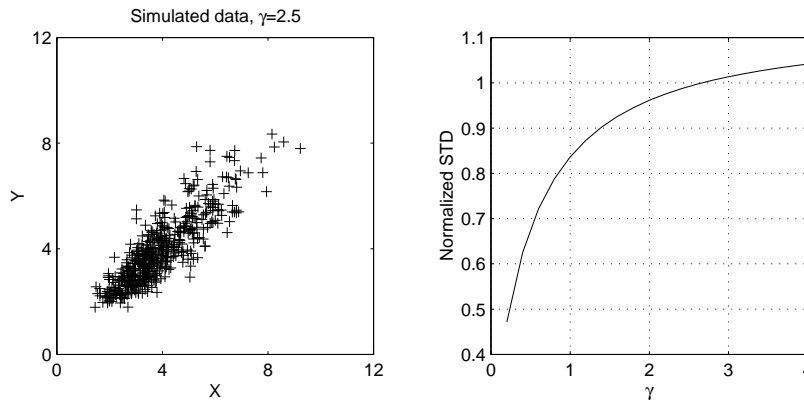


Figure 11: Estimation of gamma for simulated data where the relative error for X is 15% and 6% for Y . $N = 500$ independent samples.

It is, in fact, even possible to use Eqn. 87 to obtain an *estimate* of γ if the variance of X is known. The linear TLS for a constant γ is simple to compute, and the regression line may therefore be obtained for a series γ -s. The idea is to compute the corresponding standard deviations of $\{Z_n\}$, plot them as a function of γ , and observe where the graph crosses 1. Two examples are shown on figures 10 and 11. Judging from the graphs, it seems that the correct γ is found quite correctly, although a γ less than 1 seems to be spotted more accurately than a γ larger than one.

This idea has not been found in the literature, but should certainly be known. It is clear that deviation from a strict linear relationship and estimation errors in α and β will influence the conclusions.

5.3 Nonparametric Techniques

Nonparametric techniques are interesting in a situation where little is known about the regression between the data we are intercomparing. Also, non-parametric techniques may be used for a first inspection of the data, e.g. for checking a linear relationship. Most non-parametric regression seems to assume no error in one of the variables, a notable exception is the book of Carroll, Ruppert and Stefanski [10]. However, even non-parametric error-in-variable models [11] tend to assume a more simple error behaviour than we have here.

5.3.1 Quantile plots as a non-parametric regression

There is a very simple and direct way of obtaining a completely non-parametric regression function $Y = h(X)$ between two arbitrary wave parameters X and Y from their respective empirical cumulative distribution functions, F_X and F_Y .

The technique is known as the *Quantile-Quantile (Q-Q) plot* and is commonly used to for inspecting whether a given set of data follows some specified distribution. We recall that the quantile x_q for X is the value such that $F_X(x_q) = q$. Since this application may also be of interest in our setting, we consider it first. For an observed data set, $\{X_n\}_{n=1}^N$, let $X_1^* \leq X_2^* \leq \dots \leq X_N^*$ be the corresponding ranked observations and $F(x)$ the theoretical cumulative distribution function of the specified model. The Q-Q plot consists of the graph of the pairs $\{X_n^*, F^{-1}((n - \frac{1}{2})/N)\}$. This is actually a comparison of the cumulative distribution functions: If the empirical distribution function of the observations follows the theoretic distribution, the plot will show something close to a straight line. However, in order to really test whether an observed off-set is really statistically significant, it is necessary to carry out a test, e.g., the well-known Kolmogorov-Smirnov test on the presumably uniformly distributed variable $F(X)$.

By replacing exact distribution with an other empirical distribution belonging to the variable Y , we obtain a Q-Q plot, which in effect is a non-parametric regression curve. This can be seen as follows. Let us disregard the sampling variability and assume that there is a monotonely increasing calibration function between the observations of the underlying wave parameter, μ , such that $x = \mu$ and $y = h(\mu)$. Since h is monotone,

$$F_X(x) = P(X \leq x) = P(h(X) \leq h(x)) = F_Y(h(x)), \quad (90)$$

from which it follows that

$$y = h(x) = F_Y^{-1}(F_X(x)). \quad (91)$$

The calibration function may thus be expressed by the cumulative distribution function. In fact, for an observed data set $\{x_n, y_n\}$, $n = 1, \dots, N$, the piecewise linear function defined by the ranked observations, $x_1^* \leq x_2^* \leq \dots \leq x_N^*$ and $y_1^* \leq y_2^* \leq \dots \leq y_N^*$, will be a simple estimate of h . The same idea may also be used if the number observations between X and Y are not the same. Fig. 12 shows an example where Q-Q regression is used for an intercomparison between HF radar and buoy measurements from the Dutch coast [30]. The straight lines are linear ML regressions (close to TLS lines). Although the non-parametric and the ML regression coincide exactly for the bulk of the measurements, the deviation in the upper part is quite obvious and discussed further in the paper.

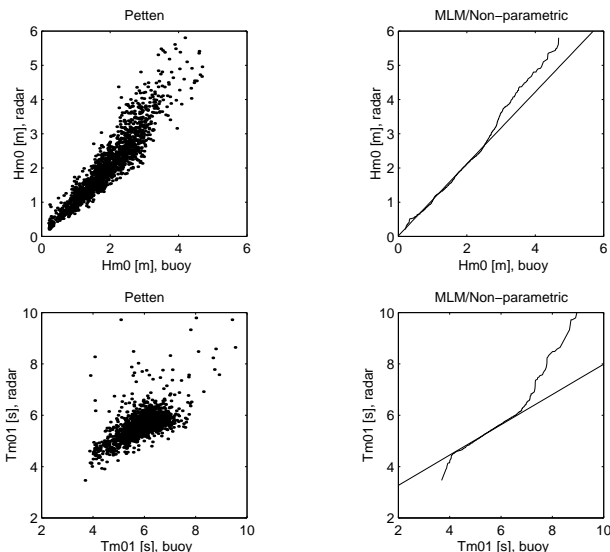


Figure 12: Example of Q-Q-regression compared to linear ML-regression. The data are from the SCAVVEX project (Wyatt et al. 1999).

Since sampling errors ”stretch” the sampling distributions compared to the exact distributions, this will introduce some bias if the sampling error is large compared to the underlying variation of the variables, or if the sampling errors are highly different for X and Y . This is demonstrated for simulated data in Fig. 13 In these data, the variance is defined by

$$V = (0.1 \cdot x)^2,$$

$$\text{Var}(X) = V\sqrt{\gamma}, \text{Var}(Y) = V/\sqrt{\gamma}.$$

There are several ways to correct for the bias. The simplest way would simply be to add artificial independent error in the variable with the least error so as to make $\gamma \approx 1$. A similar idea for many different situations are suggested in [10]. However, this results in an additional smearing of the true probability density of the variable. The ideal solution would however be to *deconvolve* the empirical distributions before the Q-Q-plot is formed. Deconvolution techniques are briefly described in [10], but methods based on the characteristic function or moment fit are not applicable here, since the error variance typically depend on value of the variable itself. Thus the density of X is not simply a convolution between the density of π and the density of the error. It should be possible to apply some of the inverse problem deconvolution methods (vanCittert or Landweber iteration), but application of those to the present case is not known.

6 Intercomparison of Directional Spectra

Due to the large dynamic range of directional spectra, together with considerable sampling variability, direct comparisons using contour or 3D plots are not completely straightforward. Often spectra are shown auto-scaled with respect to the maximum, – a value with considerable random scatter. The simple compromise is often to plot frequency dependent parameters like the mean

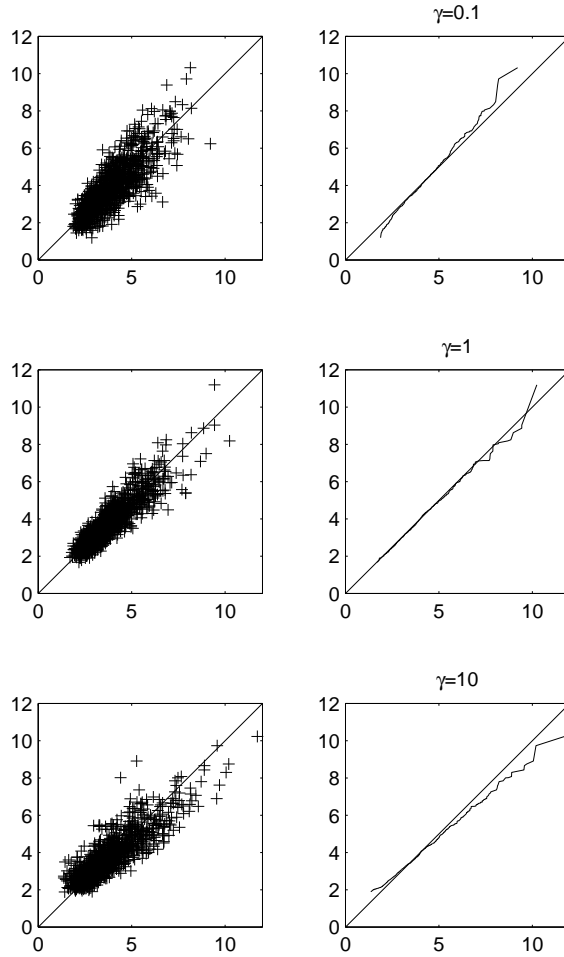


Figure 13: Simulated data sets ($N = 1000$) and the corresponding Q-Q-regressions. When γ deviates significantly from 1, this introduces considerable bias in the curve, and is even slightly visible in the scatter plots.

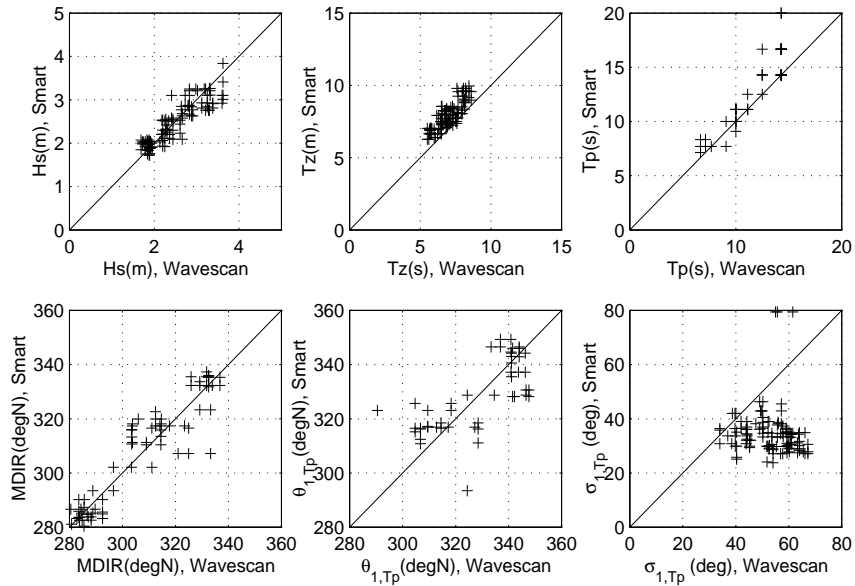


Figure 14: Comparison of a selection of wave parameters from the Smart-800/Wavescan sea trials. Note the expanded directional scale for the main and mean directions.

direction and the directional spread superimposed on plots similar to superimposed frequency spectra. This is quite informative as long as we only have one dominant wave field, but for complicated multi-modal situations in the same frequency band, the mean direction and directional spread may be quite meaningless.

The solution is probably that intercomparison of directional spectra should be carried out using *partitioned* spectra. A brief review of current spectral partitioning algorithms is included below.

6.1 Conventional Intercomparisons

Figure 14 shows a typical intercomparison using overall wave parameters for two different buoy systems (The Smart and Wavescan Buoys) [5]. Whereas significant wave height, peak period and the main and mean directions show reasonable agreement, the mean wave period is biased and the directional spread around the spectral peak is significantly lower for the Smart buoy. The difference in wave period was in this case explained from an intercomparison of the spectra, where it was found that the spectral ratio $S_{Smart}(f)/S_{WSC}(f)$ drops from one around the most energetic parts of the spectra to about .5 in the high frequency end at 0.4Hz. The reason is probably caused by different hydrodynamic response for the two buoys. The difference for the directional spread is also observed in the more smeared appearance of the Wavescan spectra as shown in Fig. 15, and the explanation has been traced back to the Wavescan compass reading.

In general, intercomparison of directional spectra is complicated since the spectra themselves may be quite complex, as the example in Fig. 16 shows. In this case, however, the agreement is excellent, but if some of the fields have been slightly shifted in frequency and direction, say if one spectrum has been a model spectrum, the only way to assess differences would be to partition the

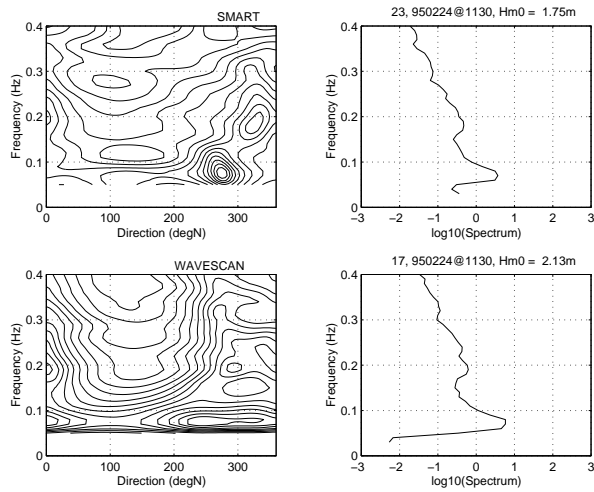


Figure 15: Intercomparison of directional spectra from the Smart (upper) and Wavescan (lower) buoys. Note the more smeared appearance of the Wavescan spectrum.

spectra before the intercomparison proceeds.

6.2 Spectral Partitioning

In order to effectively deal with the huge amount of information that is required to make a robust estimate of full directional ocean wave spectra, Gerling [13] devised a spectral partitioning scheme for decomposing a given spectrum into components created by uncorrelated meteorological sources. He then used the partitioned spectrum as a tool to obtain a statistical description of the wave spectrum as a superposition of independently evolving wave systems. The partitioning scheme of Gerling was later modified by Hasselmann *et al.*, [19], to give an algorithm which is better suited for wave spectra comparisons. Many authors, including [16, 17, 18, 29], has successfully shown that this scheme can effectively be used to characterize multiple distinct wave systems across space and time with a greatly reduced set of parameters.

Here we briefly outline a generalized form of Hasselmann’s partitioning scheme and discuss it’s application to comparison and assimilation of directional wave spectra data. Following Hanson and Phillips, [16], we split the partitioning algorithm into five separate steps:

1. Isolate the spectral energy peaks,
2. Identify and combine wind sea peaks,
3. Identify and combine mutual swell peaks,
4. Remove low energy partitions,
5. Calculate partition statistics.

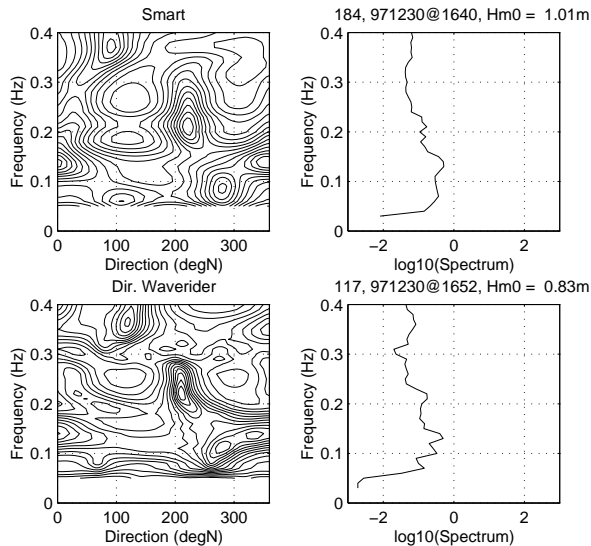


Figure 16: Simultaneous directional spectra (left) and frequency spectra (right) from the Smart and Directional Waverider buoys. Low, mixed sea state.

The output of this algorithm is thus a set of wave spectrum statistics associated with a partition of a directional wave spectrum into uncorrelated wave systems. The physical interpretation of each partition is thus that it represents a wave system originating from a certain meteorological event which is uncorrelated with the meteorological events that created the other wave systems in the partitioning sequence.

6.2.1 Isolate the spectral energy peaks

The idea behind the peak isolation procedure is analogous to the concept of a catchment area in hydrology if one considers the spectrum as an "inverted" hilly landscape. To be precise, a partition is defined as the set of all points in the polar (f, θ) plane whose steepest ascent paths lead to the same local maximum. Thus, for each local maximum we associate an "inverted" catchment area, and this inverted "valley" is a (preliminary) partition.

6.2.2 Identify and combine wind sea peaks

The next step is to isolate the locally generated wind sea peaks from the swell peaks which typically originate from distant storms. For this we use a wave age criterion: a peak is classified as wind sea if the peak wave frequency lies in the region

$$\{f \in \mathcal{R}^+ : 2\pi f \geq \gamma g [u_w \cos \delta]^{-1}\},$$

where g is the acceleration of gravity, u_w is the observed or modeled wind speed, and $\delta \in [0, \frac{\pi}{2})$ is the maximum angle between the wind and the peak direction of the propagating wind sea waves. Finally, $\gamma < 1$ is a pre-specified constant, typically in the range $[\frac{2}{3}, \frac{3}{4}]$, which ensures that all

possible wind sea peaks are included. Upon classification, all wind sea peaks are combined into one partition, say partition 0.

6.2.3 Identify and combine mutual swell peaks

Our next task is to identify which of the swell peaks, if any, that originate from the same source. These peaks must, in order to achieve a partitioning sequence of uncorrelated wave systems, be combined into one partition. The separation criteria to be used here is (a) the distance between two peaks is too small compared with the spectral spread of the respective peaks, and/or (b) the minimum spectral energy density on the "ridge" between the two peaks is too high relative to the peak energy of smaller of the two peaks.

Thus, following Hasselmann et al., [17], we convert to Cartesian coordinates

$$\xi = (f, \theta) \rightarrow (\xi_x, \xi_y) = (f \cos \theta, f \sin \theta) ,$$

denote by $\Delta(p_i, p_j) = |p_i - p_j|$ the Euclidean distance between two adjacent peaks p_i and p_j , and define the spread $\delta(p)$ of peak p according to

$$\delta^2(p) = \overline{(\xi_x - \bar{p}_x)^2} + \overline{(\xi_y - \bar{p}_y)^2} = \overline{\xi_x^2 + \xi_y^2} - (\bar{p}_x^2 + \bar{p}_y^2) .$$

Here the overbar $\bar{\cdot}$ denotes the spectral weighted average over partition $P = P(p)$, i.e.

$$\bar{\rho} = \frac{1}{e(P)} \int_P \rho dE = \frac{1}{e(P)} \int_P \rho E(f, \theta) df d\theta ,$$

where $e(P) = \int_P dE$ is the total spectral energy of partition P . We combine the two adjacent swell partitions $P(p_i)$ and $P(p_j)$ if

$$\Delta(p_i, p_j) \leq \kappa \max\{\delta(p_i), \delta(p_j)\} ,$$

for some suitable spread factor κ .

The second criteria (b) should need no further explanation.

6.2.4 Remove low energy partitions

Partitions whose total energy is very small compared to the total energy of the entire spectrum are considered to be insignificant in the sense that they do not have an important impact on any of the dominating wave systems in the spectrum. We therefore do not wish to waste time on assimilating data from these partitions. Hence, partitions with total energy below a certain energy threshold are simply removed from the partitioning sequence.

6.2.5 Calculate partition statistics

The final step is to calculate, for each of the remaining partitions, a small number of statistical parameters which capture the main characteristics of the different wave systems. The selection of parameters depends on the application.

6.3 Cross assignment of spectral wave systems

In order to be able to monitor the evolution of wave systems in space and time we need to introduce a cross assignment criterion for when two partitions of two different spectra are sufficiently similar to be classified as the same wave system. Hence, following Voorrips et al., [29] we consider two spectra A and B that have been partitioned into n_A and n_B spectra respectively. We then say that partition $i \in [1, \dots, n_A]$ of A should be cross assigned to $j \in [1, \dots, n_B]$ of B if i and j :

- are partitions of the same type (sea or swell),
- have comparable intensity: $\nu^{-1}e(i) \leq e(j) \leq \nu e(i)$, and
- are close in the spectral plane: $|\bar{f}_i - \bar{f}_j| \leq \eta_f$, $|\bar{\theta}_i - \bar{\theta}_j| \leq \eta_\theta$,

for some appropriate constants ν, η_f, η_θ . If several of the partitions of spectrum A fulfill the above requirements, then the one which is closest in wavenumber is chosen.

Clearly, it is possible that not every partition of A can be cross assigned to a partition of B . If the two spectra represent the ocean state at the "same" location in space, but at two different locations in time, then non-assigned partitions can be interpreted as newly generated wave systems or old wave systems which have faded out. However, if we are comparing model spectra with some observed or measured spectra, then the non existence of companion wave systems is more difficult to explain, and suggests that we need to adjust our model in order to achieve better coherence with the observed spectrum. A deeper discussion of how to treat non-assigned partitions in comparisons of directional wave spectra can be found in [29], Sec. 5.6.

7 Conclusions

This report has discussed some of the many questions that are met when comparing wave measurements. Few examples are included, and, in particular, more experience with non-linear and non-parametric regression should have been checked out.

In addition, the spectral partitioning seems to be a promising way when intercomparing directional spectra.

References

- [1] Abramowitz, M. and I. Stegun: *Handbook of Mathematical Functions*, Nat. Bureau of Standards, Appl. Math. Series No. 55. 10th printing, 1972.
- [2] Anderson, T. W., Estimating linear statistical relationships, *Annals of Statistics*, 1984, 12,1, pp. 1–45.
- [3] Allender, J. , T. Audunson, S.F. Barstow, H.E. Krogstad, S. Bjerken, P. Steinbakke, L. Vartdal, L.E. Borgman, C. Graham: The WADIC Project: A Comprehensive Field Evaluation of Directional Wave Instrumentation, *Ocean Engineering*, Vol.16 (1989) pp 505–536.

- [4] Barstow, S.F., H.E. Krogstad, K. Torsethaugen, and T. Audunson: Procedures and problems associated with the calibration of wave sensors, *Adv. Underw. Techn. and Offs. Eng.*, Vol. 4 (1985) pp. 55–82.
- [5] Barstow, S.F. and H.E. Krogstad, Intercomparison of directional wave sensors and buoys, in *Directional Wave Spectra*, EU COST Action 712, to be published.
- [6] Boggs, P.T., R.H. Byrd, and R.B. Schnabel: A stable and efficient algorithm for nonlinear orthogonal distance regression, *SIAM Sci. and Stat. Comp.*, Vol. 8, No. 6, (1987) pp. 1052–1078.
- [7] Boggs P.T. and J.E. Rogers: Orthogonal Distance regression, *Cont. Mathematics*, Vol. 112: *Statistical Analysis of Measurements Error Models and their Applications* (Ed. P.J. Brown and W.A. Fuller), 1990, pp. 183–194.
- [8] Brillinger, D.R.: *Time series: Data Analysis and Theory*, Holt, Rinehart and Winston, New York, 1975.
- [9] Capon, J.: Maximum likelihood spectral estimation, in Nonlinear Methods in Spectral Analysis, *Topics in Applied Physics*, Vol. 34, ed. S. Heykin, Springer, Berlin, Heidelberg, New York (1969) pp.155–179.
- [10] Carroll, R.J, D. Ruppert, and L.A. Stefanski: *Measurement Error in Nonlinear Models*, Chapman & Hall, 1995.
- [11] Fan and Truong: Nonparametric regression with errors in variables, *Ann. Stat.*, Vol. 21, No. 4 (1992) pp. 1900–1925.
- [12] Fuller, W. A.: *Measurement Error Models*, Wiley, 1987.
- [13] Gerling, T.W.: Partitioning sequences and arrays of directional wave spectra into component wave systems, *J. Atmos. Oceanic Technol.*, 1992, **9**: 444-558.
- [14] Glad, I.K.: *Statistiske estimatorer til estimatorer for bølgeretningsestimatorer*. Master thesis (In Norwegian), NTH, April 1990.
- [15] Guillaume, A. : Statistical tests for the comparison of surface wave spectra with applications to model validations, *J. Atmos. Ocean. Tech.*, Vol. 7 (1990) pp. 557–567.
- [16] Hanson, J.L. and O.W. Phillips: Automated analysis of ocean surface directional wave spectra, *J. Atmos. Oceanic Technol.*, 2001, **18**: 277-293.
- [17] Hasselmann, S., C. Brüning, K. Hasselmann, P. Heimbach, An improved algorithm for the retrieval of ocean wave spectra from synthetic aperture radar image spectra, *J. Geophys. Res.*, 1996, **101**(C7): 16,615-16,629.
- [18] Hasselmann, S., P. Lionello, K. Hasselmann, An optimal interpolation scheme for the assimilation of spectral wave data, *J. Geophys. Res.*, 1997, **102**(C7): 15,823-15,836.

- [19] Hasselmann S., K. Hasselmann, C. Brüning, Extraction of wave spectra from SAR image spectra, in *Dynamics and Modeling of Ocean Waves*, G. Komen (ed.), Cambridge Univ. Press, Cambridge, England, 1994: 391-401.
- [20] Komen, G., L. Cavaleri, M. Donelan, K. Hasselmann, S. Hasselmann, P.A.E.M. Janssen, *Dynamics and modeling of ocean waves*, Cambridge Univ. Press, New York, 1994.
- [21] Krogstad, H.E: On the Covariance of the Periodogram, *J. Time Series Analysis*, Vol. 3 (1982) pp. 195-207.
- [22] Krogstad, H.E., J. Wolf, S.P. Thompson and L. R. Wyatt: Methods for Intercomparison of Wave Measurements, *Coastal Eng.*, Vol. 37 (1999) pp. 235–257.
- [23] Long, R. B.: The statistical evaluation of directional spectrum estimates derived from pitch/roll buoy data, *J. Phys. Ocean.*, Vol. 10 (1980), pp. 944–952.
- [24] Mardia, K. V.: *Statistics of directional data*, Academic Press, 1972.
- [25] Munthe-Kaas, H. and H.E. Krogstad: *Sampling variability of sea state parameters*, ANODA Report no. 09, SINTEF (1985).
- [26] Samset, O., H.E. Krogstad, and O. Haug: *Analysis of Holderness data: A comparison between directional waverider and the OSCAR HF radar data*, SCAWVEX Technical report, SINTEF (1996)
- [27] Sova, M.S.: *The Sampling Variability and the Validation of High Frequency Wave Measurements of the Sea Surface*, Univ. of Sheffield PhD Thesis (1995a).
- [28] Tucker, M.J.: Recommended standard for wave data sampling and near real-time processing, *Ocean Engineering*, 20, (1993) pp. 459–474.
- [29] Voorrips, A.C., V.K. Makin, S. Hasselmann, Assimilation of wave spectra from pitch-and-roll buoys in a North Sea wave model, *J. Geophys. Res.*, 1997, **102**(C3): 5829-5849.
- [30] Wyatt, L.R., S.P. Thompson and R.R. Burton: Evaluation of HF radar wave measurements, *Coastal Engng*, 1999, **37**, pp. 259–282.
- [31] Willmott C.J. , S.G. Ackleson, R.E. Davies, J.J. Feddema, K.M. Klink, D.R. Legates, J. O’Donnell and C.M. Rowe: Statistics for Evaluation and Comparison of Models, *J. Geophys. Res.*, Vol. 90 (C5) (1985) pp. 8995–9005.